# Assessment of thermodynamic data for CuCrO$_2$ delafossite from calorimetric measurements

J. Schorne-Pinto[a,b], A. Janghorban[c], M. Lomello-Tafin[c], A. Pisch[d], G. Mikaelian[e], P. Benigni[e], A. Barnabé[b], L. Cassayre[a,*]

[a] *Laboratoire de Génie Chimique, Université de Toulouse, CNRS, INP, UPS, Toulouse, France*
[b] *CIRIMAT, Université de Toulouse, CNRS, UT3 - Paul Sabatier, 31062 Toulouse Cedex 9, France*
[c] *Laboratoire SYMME, Université Savoie Mont Blanc, Annecy, France*
[d] *SIMAP, UGA/CNRS/Grenoble INP, 38000 Grenoble, France*
[e] *Aix Marseille Univ., Univ. Toulon, CNRS, IM2NP Marseille, France*

A B S T R A C T

A detailed investigation of the thermodynamic properties of delafossite CuCrO$_2$ was carried out by experimental methods on synthetic CuCrO$_2$ delafossite samples (differential scanning calorimetry from ambient to 871 K and drop calorimetry from 823 to 1123 K) and theoretical methods (density functional theory). Based on these data and available literature (low temperature heat capacity measurements and calculations, high temperature *emf* data), we propose, for the first time, a full set of thermodynamic data for the phase CuCrO$_2$. Our selection comes to: $\Delta_f H°_{298}(CuCrO_2) = -670.8 \pm 1.3 \, \mathrm{kJ \, mol^{-1}}$, $S°_{298}(CuCrO_2) = 88.9 \, \mathrm{J \, K^{-1}}$, and $c_p°$ $(T) = 1.02564 \cdot 10^2 - 2.87159 \cdot 10^7 \, T^{-3} - 1.28542 \cdot 10^5 \, T^{-1.5}$ (298 < T < 1300 K).

## 1. Introduction

Cuprous delafossite type oxides Cu$^{1+}$M$^{3+}$O$_2$ with M = (Cr$^{3+}$, Fe$^{3+}$, Al$^{3+}$, among others) have been a topic of intense scientific activity over the last two decades due to their unique physical and chemical properties. Among them, the cuprous chromite CuCrO$_2$, also named "Mac Connellite" in its mineral form and sometimes noted as Cu$_2$Cr$_2$O$_4$ in older works, is one of the most promising candidates for transparent p-type conducting oxide in optoelectronic devices [1–3]. This compound is also of interest for its catalyst/photocatalytic [4,5] and thermoelectric applications [6–8]. Moreover, the CuCrO$_2$ phase presents remarkable physical properties such as multiferroic behavior [9,10] at low temperatures.

The CuCrO$_2$ delafossite crystallizes with the rhombohedral structure (space group R$\overline{3}$m) composed of alternating layers of linearly coordinated O-Cu$^{1+}$-O and Cr$^{3+}$O$_6$ edge-shared octahedra. In air, this phase is stable from 1073 K [4] up to a temperature higher than 1833 K based on observations of a quenched sample by Gadalla et al. [11]. This phase is one of the three mixed oxide (together with the CuCr$_2$O$_4$ spinel and CuCrO$_4$ copper chromate [12,13]) composing the Cu-Cr-O ternary system, in which Hamuyuni and Taskinen recently performed liquidus measurements [14].

However, limited thermodynamic data for CuCrO$_2$ are available in the literature. As evidenced by Perrot in his review of the Cu-Cr-O system in 2010 [15], there is a strong lack of experimental information such as heat capacity, entropy, and enthalpy for CuCrO$_2$, at room temperature and above. At high temperature, two systematics studies were performed on the Cr-Cu-O system by *emf* method. Jacob et al. [16] reported information on mixed oxides CuCrO$_2$ and CuCr$_2$O$_4$ in addition to the single oxides Cr$_2$O$_3$, CuO, and Cu$_2$O in the 900–1350 K temperature range. The same year, Vlach et al. [17] performed similar measurements, and included an extensive review of Gibbs energy values for the formation reaction of CuCrO$_2$. Among the twelve studies they reported for the CuCrO$_2$ phase, their *emf* values, the values of Jacob et al. [16] and the derived function obtained by Schmahl and Minzl [18] are in good agreement. The applicative interest of the CuCrO$_2$ phase also favored studies of the low-temperature heat capacity, magnetization, and resistivity. Indeed, Okuda et al. [19] made estimations of the heat capacity between 0 to 150 K, and Poienar et al. [20] carried out heat capacity measurements between 2.5 and 50 K. Finally, a value for the enthalpy of formation of the phase at 0 K was proposed by Scanlon & Waston [21], based on density functional theory (DFT) calculations.

Due to some lack of experimental data, especially for the heat

---

* Corresponding author.
  *E-mail address:* laurent.cassayre@ensiacet.fr (L. Cassayre).

capacity between 150 and 1000 K, no thermodynamic functions were proposed so far for the $CuCrO_2$ delafossite phase. In this work, we performed heat capacity measurements with differential scanning calorimetry (DSC) from ambient temperature to 871 K and drop calorimetry from 823 to 1123 K on synthetic $CuCrO_2$ delafossite samples, as well as DFT calculations at 0 K. Then, we assessed a full set of refined thermodynamic data from 298.15 K (which will be noted 298 K in the rest of the paper) to 1300 K, based on a third law analysis of our data and literature data, following a similar procedure as presented by Jacob et al. [22] for the MnO phase.

## 2. Materials and methods

### 2.1. Preparation and characterization of $CuCrO_2$ samples

#### 2.1.1. Polycrystalline powder synthesis

$CuCrO_2$ was prepared by high-temperature solid-state reaction in nitrogen atmosphere as described elsewhere [23]. The $Cu_2O$ (Alfa Aesar 99%) and $Cr_2O_3$ (Acros Organics, 99 + %) powders were mixed in stoichiometric quantities in a mortar and then treated at 900 and 1000 °C for 30 h, with intermediate grindings to ensure good homogeneity.

#### 2.1.2. Sintering & pellets preparation

Resulting powder was mixed with an organic binder (Rhodoviol®) and uniaxially pressed into a pellet of 2 cm in diameter. The debinding was carried out under air at 400 °C, and the sintering at 1050 °C with a dwell time of 10 h under Ar atmosphere.

#### 2.1.3. Composition analysis

The cationic molar ratio of the $CuCrO_2$ product was checked by Field Emission Gun - Electron Probe Microanalysis FEG-EPMA (SX Five FE, CAMECA) before and after drop calorimetry. X-Ray Fluorescence spectroscopy (XRF) (S2 Ranger, Bruker) was also performed to confirm the composition.

#### 2.1.4. Structural analysis

The pellets were characterized before and after drop calorimetry by room-temperature X-Ray Diffraction (Bruker D 4 d iffractometer, λCu Kα1 = 1.54056 Å and Kα2 = 1.54443 Å radiation).

#### 2.1.5. Cutting samples

Cuboid samples of around 40 mg ($\approx 3 \times 3 \times 3$ mm$^3$) were obtained by cutting the initial pellet using a wire saw.

### 2.2. Drop calorimetry: apparatus and procedure

An isothermal Multi-HTC calorimeter from Setaram Instrumentation was used for this study. The calorimetric cell was heated by a vertical furnace and connected to an atmosphere controlled-tight container, loaded alternately with alumina pieces and $CuCrO_2$ cuboid samples. The experiments were done in an alumina crucible containing a one-centimeter-thick bed of $HfO_2$ powder in order to ensure the best reproducibility of heat transfers. The drop measurements were performed in flowing argon (99,999% N50) having an impurity of $O_2$ less than 2 ppm, that leads to a maximal value of oxygen partial pressure of $2.10^{-6}$ atm. The temperature was calibrated with respect to pure standard metals (Al, Ag, Au). Their melting temperature was recorded at three heating rates (1, 2.5 and 5 K min$^{-1}$) and were linearly extrapolated to zero heating rate. The calibration of the calorimeter was achieved by dropping an alumina sample into the crucible before and after each drop of $CuCrO_2$ sample. The sensitivity of the calorimetric cell was determined by comparing the calorimetric signals with tabulated data for $Al_2O_3$ [24]. The temperature of the Ar-tight container was measured using an individual thermometer prior to each drop. The cell temperature had a fluctuation range between ± 0.01 K and ± 0.03 K as

the isotherms increased from 823 K to 1123 K. The thermopile fluctuations for all isotherms was found to be less than ± 1.6 μV. The baseline treatment and the peak integration were done with the CALISTO Setaram software.

### 2.3. DSC: apparatus and procedure

The DSC 111 instrument and the procedure used for measuring the heat capacity of $CuCrO_2$ are the same as used for ZnSb and described in [25]. Further relevant experimental details are described in this section.

A mass of 114.220 mg of $CuCrO_2$ powder was weighed with a microbalance ( ± 1 μg), and hermetically sealed in a first stainless steel crucible under argon within a glovebox. Then, a mass of 68.345 mg of Standard Reference Material SRM720 α-$Al_2O_3$ [24] was sealed in a second stainless steel crucible, and finally, two other similar crucibles were sealed empty. The four crucibles of equal weights were all sealed inside the glovebox, in which the oxygen level was lower than 2 ppm, and the water level was measured at 53 ppm using a cermet hygrometer.

The heat capacity was measured between 300 and 871 K using the small temperature step method. The three parameters of the temperature program were as follows: temperature step of 2.5 K, heating rate of 1.5 K min$^{-1}$ between each step and stabilization time of 800 s after each temperature step.

The heat capacity measurement by DSC requires three consecutive heating runs: the so-called zeroline, calibration, and sample runs as detailed in [25]. To protect the steel crucibles from possible oxidation during these runs, the experiments were performed under a flow of argon gas, Alphagaz 1 commercial grade (purity > 99.999% vol., $O_2$ < 2 ppm, $H_2O$ < 3 ppm, $C_nH_m$ < 0.5 ppm) supplied by the Air Liquide company. Before starting the temperature program, the two tubes of the differential calorimeter were flushed with an argon flowrate of approximately 0.5 L min$^{-1}$ during 1 h. This argon flowrate was maintained during the whole duration of the experiments.

The temperature measurement within the DSC device was calibrated with respect to the melting temperature of pure In, Sn, Zn, and Al.

### 2.4. Theoretical methods

The ground state properties of $CuCrO_2$ were calculated using DFT [26,27]. The calculations were performed using the VASP software package [28,29] in its most recent version (5.4.4).

The many-body exchange semi-local density functional SCAN (Strongly Conditioned and Appropriately Normed) [30] was used to compute the ground state properties of $Cu_2O$, $Cr_2O_3$, and $CuCrO_2$. For Cu and Cr, the 3d and 4s orbitals and for O the 2s and 2p orbitals are considered as valence states in the calculations. The energy cut-off for the projector augmented plane-wave bases was set to 800 eV. An automatically generated, gamma centred grid of k-points in the irreducible part of the Brillouin zone was used following the Monkhorst-Pack scheme [31]. The k-point grid for $Cu_2O$ was $11 \times 11 \times 11$, for $Cr_2O_3$ $7 \times 7 \times 7$ and for $CuCrO_2$ $11 \times 11 \times 2$. The magnetic properties for $Cr_2O_3$ (antiferromagnetic) and $CuCrO_2$ (ferromagnetic) were taken into account.

The lattice parameters for all three solids as well as the internal atomic coordinates were fully relaxed. The linear tetrahedron method with Blöchl corrections [32] was used to calculate the electronic Density of States (DOS). The relaxations were performed with a convergence criterion of $10^{-8}$ eV Å$^{-1}$ for the total energy and $10^{-6}$ eV Å$^{-1}$ for the forces to avoid any kind of residual stress in the Hellman-Feynman forces.

The energy of formation at 0 K for $CuCrO_2$ with respect to the simple oxides was calculated using the relation:

$$\Delta E(CuCrO_2, 0 K) = E(CuCrO_2, 0 K) - 0.5 \times E(Cu_2O, 0 K) - 0.5 \times E(Cr_2O_3, 0 K) \quad (1)$$

**Table 1**
Selected thermodynamics functions and data.

| Phase | T (K) | $\Delta_f H°_{298}$ (J mol$^{-1}$) | $S°_{298}$ (J mol$^{-1}$) | $c_p°$ (J K$^{-1}$ mol$^{-1}$) | reference |
|---|---|---|---|---|---|
| Cu(fcc) | 0–298 | 0 | 33.15 | tabulated data | [38] |
| | 298–1358 | | | $24.112392 + 0.00531368\,T - 104956\,T^{-2} - 7.75338.10^{-7}\,T^2$ | SGTE database [39] |
| Cr(bcc) | Magnetic properties: $T_c = -311.50$; $B_{mag} = -0.008$ | | | | |
| | 0–298 | | | tabulated data | [40] |
| | 298–2130 | 0 | 23.54 | $26.908 - 0.0037887\,T - 278\,500\,T^{-2} - 8.86326.10^{-6}\,T^2$ | SGTE database [39] |
| O$_2$(g) | 0–298 | | | tabulated data | [41] |
| | 298–1000 | 0 | 205.03 | $22.271 + 0.0203955\,T + 153\,460\,T^{-2} - 7.94215.10^{-6}\,T^2$ | SGTE database [39] |
| | 1000–3300 | | | $33.6273 + 0.00238319\,T - 1051620\,T^{-2} - 8.1372.10^{-8}\,T^2$ | SGTE database [39] |
| Cu$_2$O(s) | 0–120 | | | experimental data | [35] |
| | 120–298 | | | experimental data | [36] |
| | 298–900 | $-170\,707$ | 92.36 | $105.25185 + 0.008024\,T - 233\,211\,481.485\,T^{-2} + 19\,262.79\,T^{-1} - 1\,569.352\,T^{-0.5}$ | FToxid database [37] |
| | 900–1517 | | | $1\,543.43089 - 0.09489\,T - 233\,221.485\,T^{-2} + 1\,838\,574.12\,T^{-1} - 94\,003.995\,T^{-0.5}$ | FToxid database [37] |
| Cr$_2$O$_3$(s) | Magnetic properties: $T_{Néel} = -306$ ; $B_{mag} = 1.938$ | | | | |
| | 0–298 | $-1\,127\,120$ | 84.77 | experimental data | [33] |
| | 298–3000 | | | $121.44 + 0.0078\,T - 2\,000\,000\,T^{-2} + 3.10^{-7}\,T^2$ | FToxid database [37] |

### 2.5. Selected thermodynamic data and functions

Thermodynamic data and functions for all pure compounds considered in this work (Cu(fcc), Cr(bcc), O$_2$(g), Cr$_2$O$_3$(s) and Cu$_2$O(s)) are compiled in Table 1. We have selected tabulated or experimental data for heat capacity below 298 K, and polynomial functions above 298 K. For Cr$_2$O$_3$(s), the low temperature heat capacity was taken from recent measurements from [33]. For Cu$_2$O(s), according to the recommendations of NIST-JANAF [34], we selected the data from [35] for $0 < T < 120$ K and from [36] for $120 < T < 298$ K. For these two single oxides, the polynomial regression are from FTOxid [37], which reproduces tabulated data recommended by NIST-JANAF [34] for $T > 298$ K.

## 3. Results

### 3.1. Structural and chemical characterizations

The sintered sample was checked by room temperature XRD that confirmed the presence of the CuCrO$_2$ single phase, without any secondary phase, with rhombohedral structure (3R polytype with the space group R$\overline{3}$m) as illustrated on Fig. 1. Based on Rietveld refinement (R factor of 4.54), the lattice parameters are a = 2.9730(3) Å and c = 17.086(2) Å.

EPMA analysis was also carried out on a cross section of a polished sample. The average composition determined by ten random point analyzes is 24.0(7) mol% of copper, 24.5(5) mol% of chromium and 51.4(6) mol% of oxygen, which corresponds to the stoichiometric composition CuCrO$_2$.
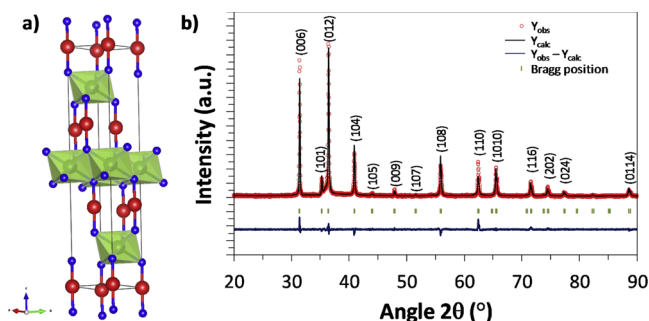


**Fig. 1.** a) Crystal structure of CuCrO$_2$, octahedron occupied by Cr$^{3+}$ and Cu$^{1+}$ in linear coordination. b) X-ray diffractogram of the sintered CuCrO$_2$ sample.



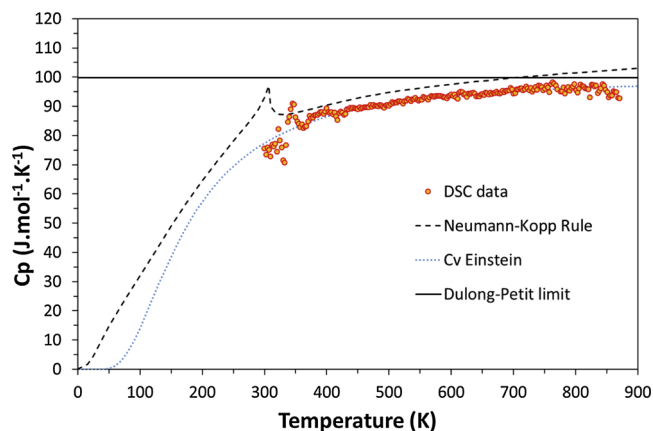**Fig. 2.** Heat capacity obtained from DSC measurements on CuCrO$_2$ sample compared to NKR, Cv from Einstein relation and the Dulong-Petit limit.

### 3.2. DSC data

The DSC data are plotted vs. temperature on Fig. 2 (numeric values are provided in the supplementary Excel file). The data are compared to an estimation of the heat capacity using the Neumann-Kopp additivity Rule (NKR) [42] established with the Cr$_2$O$_3$ and Cu$_2$O heat capacities reported in Table 1. The heat capacity at room temperature was also estimated by Dulong-Petit limit (99.77 J mol$^{-1}$ K$^{-1}$), defined as 3nR, where n is the number of atoms by molecule (n = 4) and R is the gas constant. The molar heat capacity at constant volume $c_V$ calculated with Einstein's relation (see for instance the recent work of Zienert and Fabrichnaya [43] for mathematical expression) is also reported.

The calculated NKR curve shows a kink around 320 K which is a pure artefact resulting from the magnetic transition of Cr$_2$O$_3$. Indeed, the delafossite CuCrO$_2$ phase only exhibits a magnetic transition at around 24 K according to [44] and no other transition is expected at 320 K.

Hence, the reason for the increased scattering of the experimental data points between 300 and 400 K is not fully understood. It is possibly due to vaporization of residual water, as the atmosphere of the glovebox contained 53 ppm of water when the DSC crucibles were sealed. In the 400–770 K, the DSC signal is smoother. Some scattering above 770 K might be related to the slow decomposition of CuCrO$_2$ caused by the low oxygen partial pressure in the crucible.

### 3.3. Drop calorimetry data

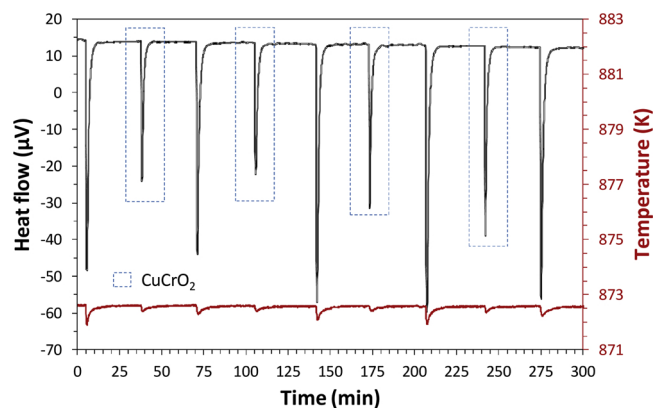An example of heat flow recorded at 872 K is provided on Fig. 3.

**Fig. 3.** Heat flow measured during successive drops of $Al_2O_3$ and $CuCrO_2$ samples at 872 K.

As indicated in the Guide to the Expression of Uncertainty in Measurement (GUM) [45], which remains the reference document related to uncertainty measurement, the nature of certain measurement procedures or tests can make the rigorous application of the GUM difficult. In our case, several sources of uncertainty contribute to a global component when enthalpy increments are measured by drop calorimetry. Then, all effects can be regarded as being addressed by estimating the overall uncertainty of the experimental values. However, each experiment must include sampling, accuracy of the instrument, preparation and analysis. Here, the standard uncertainty (u) is generally evaluated from the experimental standard deviation (s) on the data set, assuming that the increment enthalpy values follow a normal distribution. Typically, in that case, the standard uncertainty (u = s/√n) is multiplied by a coverage interval factor k = 2 to express the expanded uncertainty (U) with a confidence level of 95%. But it should be noted that this treatment is valid for an infinite number of trials only. Because our values are obtained from the average of a maximum of four measurements, we have applied the Student's coverage factor ($t_{\nu,p}$), which depends on the degree of freedom ($\nu$ = n-1) for a number of n tests and on the confidence level (p) of the coverage gap taken at 95%.

The values of the enthalpy increments at fixed temperature T ($H°_T - H°_{298}$) compiled in Table 2 are thus given with a confidence

**Table 2**
Experimental data from drop calorimetry of $CuCrO_2$ samples.

| T (K) | $H°_T - H°_{298}$ (J) | Mean (J mol$^{-1}$) | U (J mol$^{-1}$) |
|---|---|---|---|
| 823 | 46 960.1 | 47 989 | 2219 |
| 823 | 48 571.3 | | |
| 823 | 48 436.4 | | |
| 873 | 51 913.1 | 54 286 | 3555 |
| 873 | 53 552.3 | | |
| 873 | 54 423.2 | | |
| 873 | 57 254.2 | | |
| 923 | 57 856.7 | 58 621 | 1032 |
| 923 | 59 319.7 | | |
| 923 | 58 346.3 | | |
| 923 | 58 962.8 | | |
| 973 | 60 342.4 | 61 032 | 4806 |
| 973 | 65 208.9 | | |
| 973 | 60 594.2 | | |
| 973 | 57 983.7 | | |
| 1 023 | 66 552.2 | 68 676 | 4646 |
| 1 023 | 70 081.8 | | |
| 1 023 | 69 394.9 | | |
| 1 073 | 70 354.9 | 69 792 | 14 019 |
| 1 073 | 63 884.1 | | |
| 1 073 | 75 135.5 | | |
| 1 123 | 85 848.0 | 81 445 | 16 352 |
| 1 123 | 84 614.7 | | |
| 1 123 | 73 872.8 | | |
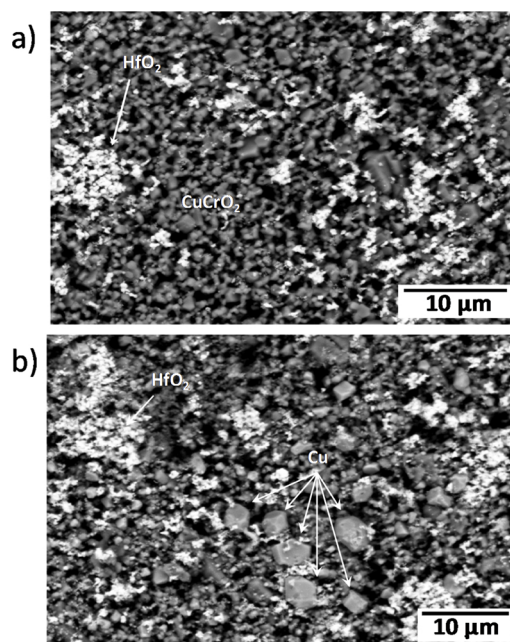


**Fig. 4.** BSE micrographs of external part of samples recovered after drop calorimetry at 1023 K (a) and 1123 K (b).

interval (U) of the mean value ($\Delta \bar{H}$) defined by:

$$H°_T - H°_{298} = \Delta \bar{H} \pm t_{\nu,p}. \frac{s}{\sqrt{n}} \qquad (2)$$

The values of the factors $t_{\nu,p}$ and the details of the estimation of the expanded uncertainties are provided in the Supplementary Excel file.

Between 823 and 1023 K, the values of the confidence intervals reported in Table 2 are about 5% of the enthalpy increments, which is fully acceptable. As illustrated in Fig. 4a, SEM-FEG characterization in BSE mode of the external part of the pellets after drop calorimetry did not evidence any modification of the pristine delafossite phase (not shown here), the presence of $HfO_2$ being attributed to some residual powder stuck to the samples.

Conversely, the confidence intervals reach 20% for the two highest temperatures (1073 and 1123 K). The XRD diffractograms of the pellets after drop calorimetry did not show any noticeable change compared to the initial material. However, SEM-FEG analyses (Fig. 4b) showed the presence of Cu metal nodules, attributed to a partial reduction of the phase during measurement caused by the low oxygen partial pressure imposed in the calorimeter. Consequently, these data were discarded in the assessment of the thermodynamic functions.

### 3.4. DFT calculations

The ground state properties (lattice parameters, total energy and magnetic moments) calculated by DFT are compiled in Table 3. The magnetic structure of $Cr_2O_3$ is antiferromagnetic with a spin sequence of + - + - along the [111] direction in the rhombohedral setting, in

**Table 3**
Ground state properties of $Cu_2O$, $Cr_2O_3$ and $CuCrO_2$.

| Phase | | $Cu_2O$ | $Cr_2O_3$ | $CuCrO_2$ |
|---|---|---|---|---|
| Lattice parameter | Å | a = 4.228 | a = 5.362 | a = 2.980 |
| | | | $\alpha$ = 54.991° | c = 17.019 |
| Magnetic moment | Bohr | – | 0 (AFM) | 8.64 (FM) |
| Ground state energy | eV fu$^{-1}$ | −37.999340 | −68.468135 | −53.443067 |
| Formation energy at | eV fu$^{-1}$ | | | −0.209330 |
| 0 K | kJ mol$^{-1}$ | | | −20.2 |

agreement with experimental data from the literature [46]. The ground state for CuCrO$_2$ is ferromagnetic with an overall magnetic moment of 8.64 Bohr.

The values of the cell parameters calculated at 0 K (a = 2.980 Å and c = 17.019 Å) are very close to the ones refined from our room temperature XRD pattern (a = 2.973 Å and c = 17.086 Å). The difference is respectively +0.10% and −0.02%, and could be attributed to the temperature dependence of the cell parameters. Indeed, these small variations are consistent with those reported by [20] from the refinement of high-resolution neutron powder diffractograms o f CuCrO$_2$, which showed a deviation of + 0.25% of a and −0.16% of c between 10 and 300 K. As a consequence, the formation energy calculated at 0 K (− 20.2 kJ mol$^{-1}$) provides an additional data that will be considered in the assessment of the thermodynamic functions of CuCrO$_2$.

## 4. Discussion

### 4.1. Temperature evolution of heat capacity from 0 to 1300 K

We have chosen to divide the evolution of the heat capacity into three temperature domains. At low temperature (T < 40 K), we selected experimental data from [20], which are consistent with simulation from [19]. Due to the occurrence of the magnetic transition, and since our major objective was to obtain an accurate entropy value at 298 K, we did not perform any fit o f t he e xperimental d ata i n this temperature range.

Above 40 K, we established two polynomial expressions, $c_p^{\circ 1}(T)$ for 40 < T < 298 K and $c_p^{\circ 2}(T)$ for 298 < T < 1300 K based on the least square method. The polynomial regression of $c_p^{\circ 1}(T)$ was established with the data from [19] for 40 < T < 150 K. The polynomial regression of $c_p^{\circ 2}(T)$ combined our experimental DSC data for 300 < T < 870 K and our experimental drop calorimetry data for 823 < T < 1023 K. The experimental drop calorimetry data $H°_T − H°_{298}$ are the reference values for the integrated $c_p^{\circ 2}(T)$ function, according to Eq. (3).

$$\int_{298}^{T} c_p^{\circ 2}(T)dT = (H°_T − H°_{298})^{calc} \tag{3}$$

The numerical resolution was constrained according to:

(i) the continuity of the two functions at 298 K : $c_p^{\circ 1}(298) = c_p^{\circ 2}(298)$
(ii) the continuity of the derivative of the two functions at 298 K :
$$\left(\frac{d\,c_p^{\circ 1}(T)}{dT}\right)_{298} = \left(\frac{d\,c_p^{\circ 2}(T)}{dT}\right)_{298}$$

The resulting polynomial functions are:

$$c_p^{\circ 1}(T) = −0.955934 + 0.383138\,T − 4.13581.\,10^{-4}\,T^2 \quad (40 < \text{T} < 298\,\text{K}) \tag{4}$$

$$c_p^{\circ 2}(T) = 1.02564.\,10^2 − 2.87159.\,10^7\,T^{-3} − 1.28542.$$
$$10^5\,T^{-1.5}\,(298 < \text{T} < 1300\,\text{K}) \tag{5}$$

The two functions are plotted in Fig. 5 together with available data. The integral of $c_p^{\circ 2}(T)$ is plotted in Fig. 6 and compared to our two set of experimental data (integrated DSC data and enthalpy increments).

### 4.2. Entropy of CuCrO$_2$ at 298 K

The entropy of CuCrO$_2$ is obtained from Eq. (6).

$$S°_{298}(CuCrO_2) = \int_0^{298} \frac{c_p^{\circ}(CuCrO_2)(T)}{T} dT \tag{6}$$

We performed direct numerical integration of the experimental values from [20] between 0 and 40 K (contribution of 9.95 J K$^{-1}$) and analytic integration of the $c_p^{\circ 1}(T)$ function (Eq. (4)) between 40 and 298 K (contribution of 78.94 J K$^{-1}$). Our recommended value for the
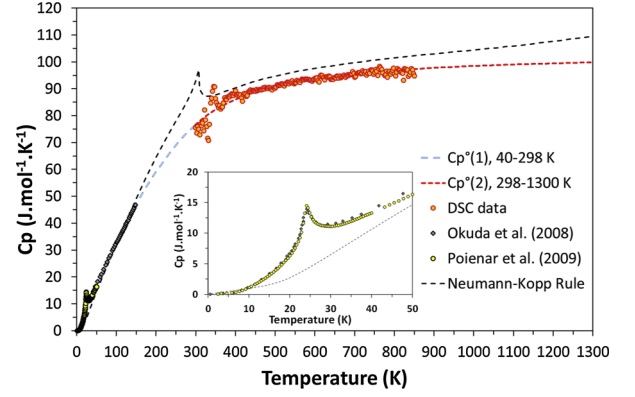


**Fig. 5.** Temperature evolution of heat capacity derived from DSC (this work), drop calorimetry (this work), low temperature calculations [19] and experimental data [20].
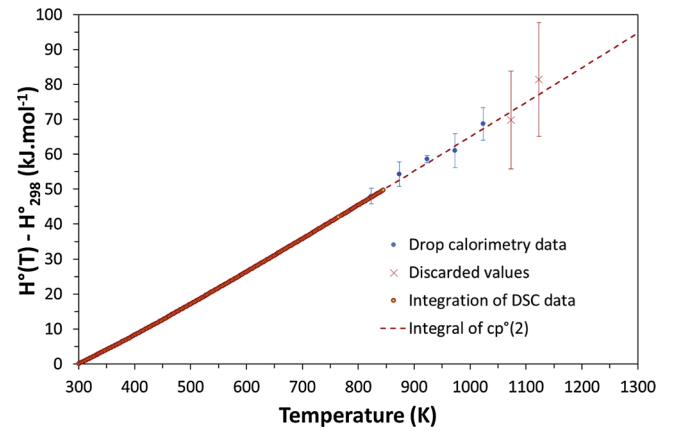


**Fig. 6.** Comparison of $\int_{298}^{T} c_p^{\circ 2}(T)dT$ with drop calorimetry data and integrated DSC data.

entropy of CuCrO$_2$ comes to: $S°_{298}(CuCrO_2) = 88.89$ J K$^{-1}$.

This value is significantly higher than the value (85.2 J K$^{-1}$) proposed by Vlach et al. [17], which was evaluated by the structural analog method using the entropy of formation of the CuFeO$_2$ delafossite. It is also slightly higher than the value (86.73 J K$^{-1}$) obtained from ideal mixing of Cu$_2$O and Cr$_2$O$_3$ (integration of Neumann-Kopp function).

### 4.3. Enthalpy of formation of CuCrO$_2$ at 298 K

The enthalpy of formation of CuCrO$_2$, $\Delta_f H°_{298}(CuCrO_2)$, is related to Eq. (7).

$$Cu(fcc) + Cr(bcc) + O_2(g) = CuCrO_2(s) \tag{7}$$
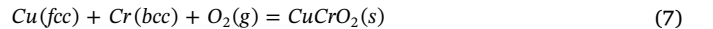
Our assessment of $\Delta_f H°_{298}(CuCrO_2)$ takes into account high temperature *emf* data from [14,15], from which we derived values of Gibbs energy of formation $\Delta_f G°_T(CuCrO_2)$.

The 14 *emf* data of [14,15] are related to the following electrochemical cell:

$$Cu_2O + Cr_2O_3 = 2\,CuCrO_2 \tag{8}$$

with $\Delta_r G°_T(cell) = −2.\,F.\,emf$
and
$\Delta_f G°_T(CuCrO_2) = \frac{1}{2}(\Delta_r G°_T(cell) + \Delta_f G°_T(Cu_2O) + \Delta_f G°_T(Cr_2O_3))$

$\Delta_f G°_T(Cu_2O)$ and $\Delta_f G°_T(Cr_2O_3)$ come from the selected thermodynamic functions compiled in Table 1. The set of 14 assessed data for $\Delta_f G°_T(CuCrO_2)$ is provided in Table 4.

For each *emf* data, a value of $\Delta_f H°_{298}(CuCrO_2)$ is obtained from Eq. (9):

**Table 4**
Reassessment of $\Delta_f\,G°_T(CuCrO_2)$ from *emf* data of [16] and [17], with selected $Cu_2O$ and $Cr_2O_3$ thermodynamic functions from Table 1.

| Data source | T (K) | *emf* (mV) | $\Delta_r\,G°_T(cell)$ (J mol$^{-1}$) | $\Delta_f\,G°_T(Cu_2O)$(J mol$^{-1}$) | $\Delta_f\,G°_T(Cr_2O_3)$(J mol$^{-1}$) | $\Delta_f\,G°_T(CuCrO_2)$ (J mol$^{-1}$) |
|---|---|---|---|---|---|---|
| [16] | 950.1 | 196.36 | − 37 889 | − 99 034 | − 879 473 | − 508 197 |
| | 953.5 | 194.08 | − 37 449 | − 98 788 | − 878 628 | − 507 433 |
| | 1000.0 | 192.71 | − 37 185 | − 95 439 | − 867 091 | − 499 858 |
| | 1068.9 | 189.07 | − 36 482 | − 90 504 | − 850 042 | − 488 514 |
| | 1143.0 | 184.51 | − 35 603 | − 85 233 | − 831 757 | − 476 296 |
| | 1237.8 | 179.50 | − 34 636 | − 78 546 | − 808 418 | − 460 800 |
| | 1339.4 | 174.03 | − 33 581 | − 71 449 | − 783 448 | − 444 239 |
| [17] | 1074.7 | 198.4 | − 38 283 | − 90 069 | − 848 535 | − 488 443 |
| | 1122.4 | 195.88 | − 37 797 | − 86 723 | − 836 934 | − 480 727 |
| | 1125.6 | 195.74 | − 37 770 | − 86 439 | − 835 948 | − 480 078 |
| | 1179.3 | 193.59 | − 37 355 | − 82 686 | − 822 888 | − 471 465 |
| | 1228.2 | 191.76 | − 37 002 | − 79 234 | − 810 829 | − 463 532 |
| | 1230.4 | 191.65 | − 36 981 | − 79 094 | − 810 337 | − 463 205 |
| | 1275.4 | 189.72 | − 36 608 | − 75 939 | − 799 272 | − 455 909 |

$$\Delta_f\,H°_{298} = \Delta_f\,G°_T - \Delta(H°_T - H°_{298}) + T(\Delta_f\,S°_{298} + \Delta(S°_T - S°_{298})) \tag{9}$$

with

$$\Delta_f\,G°_T = \Delta_r\,G°_T(CuCrO_2)$$

$$\Delta(H°_T - H°_{298}) = \int_{298}^{T} [c_p^{°2}(T) - c_p^°(Cu(fcc)) - c_p^°(Cr(bcc)) - c_p^°(O_2(g))]dT$$

$$\Delta_f\,S_{298}^° = S_{298}^°(CuCrO_2) - S_{298}^°(Cu(fcc)) - S_{298}^°(Cr(bcc)) - S_{298}^°(O_2(g))$$

$$\Delta(S°_T - S°_{298}) = \int_{298}^{T} \frac{1}{T}[c_p^{°2}(T) - c_p^°(Cu(fcc)) - c_p^°(Cr(bcc)) - c_p^°(O_2(g))]dT$$

The determination of $\Delta_f\,H°_{298}(CuCrO_2)$ is then built from (i) our assessments of $c_p^{°2}(T)$ (Eq. (5)) and $S°_{298}(CuCrO_2)$, (ii) the thermodynamic functions compiled in Table 1 and (iii) the assessed values of $\Delta_f\,G°_T(CuCrO_2)$ compiled in Table 4. As a result, we obtained 14 values of $\Delta_f\,H°_{298}(CuCrO_2)$, which are plotted as a function of the temperature of *emf* measurements in Fig. 7. Based on the average of these 14 values, our recommended value for the enthalpy of formation of CuCrO$_2$ is $\Delta_f\,H°_{298}(CuCrO_2) = -670.8 \pm 1.3\,kJ\,mol^{-1}$.

From this value of $\Delta_f\,H°_{298}$, we also derived an enthalpy of reaction corresponding to the formation of CuCrO$_2$ from the pure oxides (Eq. (8)):
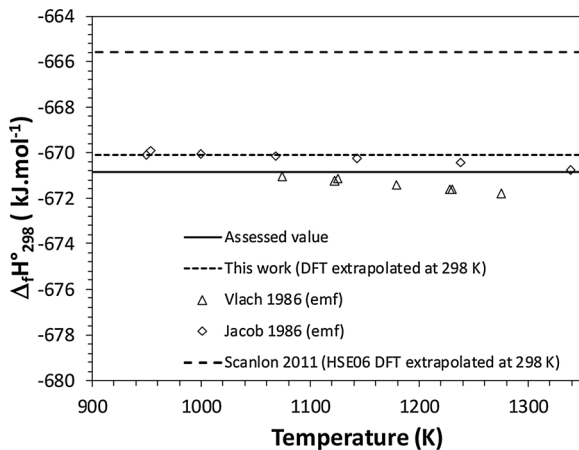


**Fig. 7.** Results of third-law analysis of Gibbs energy of formation of CuCrO$_2$; comparison to DFT calculations.

$$\Delta_r\,H°_{298}^{Ox} = \Delta_f\,H°_{298}(CuCrO_2) - \frac{1}{2}\Delta_f\,H°_{298}(Cu_2O) - \frac{1}{2}\Delta_f\,H°_{298}(Cr_2O_3) \tag{10}$$

The enthalpy value comes to $\Delta_r H°_{298}^{Ox} = -21.9 \pm 1.3\,kJ\,mol^{-1}$.

### 4.4. Comparison to DFT calculations

As reported in Table 3, our computed enthalpy of formation of CuCrO$_2$ at 0 K from single oxide compounds (1/2 Eq. (8)) is $\Delta_r H°_0^{DFT-1} = -20.2\,kJ\,mol^{-1}$. This value is compared to our assessed value at 298 K ($\Delta_r H°_{298}^{Eq2}$) using Eq. (11).

$$\Delta_r\,H°_{298}^{DFT-1} = \Delta_r\,H°_0^{DFT-1} + \int_0^{298} (\Delta c_p^°)^{R1}dT \tag{11}$$

with
$(\Delta c_p^°)^{R1} = c_p^°(CuCrO_2) - \frac{1}{2}c_p^°(Cu_2O) - \frac{1}{2}c_p^°(Cr_2O_3)$
$c_p^°(CuCrO_2)$: $c_p^{°1}(T)$ for $40 < T < 298\,K$ (Eq. (4)) and tabulated value for $0 < T < 40\,K$
$c_p^°$ data for Cu$_2$O and Cr$_2$O$_3$ from Table 1
The integral of $(\Delta c_p^°)^{R1}$ is equal to $-1.00\,kJ\,mol^{-1}$. The resulting value for $\Delta_r H°_{298}^{DFT-1}$ is $21.2\,kJ\,mol^{-1}$, which is fully consistent with $\Delta_r H°_{298}^{Ox}$.

Ab initio calculations from [21] provide another value of enthalpy of formation of CuCrO$_2$ at 0 K, from pure metals (Eq. (7)): $\Delta_f H°_0^{DFT-2} = -660.9\,kJ\,mol^{-1}$. Their value computed at 0 K is compared to our assessed value of $\Delta_f\,H°_{298}$ by extrapolation to 298 K according to:

$$\Delta_f H°_{298}^{DFT-2} = \Delta_f H°_0^{DFT-2} + \int_0^{298} (\Delta c_p^°)^{R2}dT \tag{12}$$

with

$$(\Delta c_p°)^{R2} = c_p^°(CuCrO_2) - c_p^°(Cu(fcc)) - c_p^°(Cr(bcc)) - c_p^°(O_2(g))$$

$c_p^°(CuCrO_2)$: same as Eq. (11)
$c_p^°$ data for Cu(fcc), Cr(bcc) and O$_2$(g) from Table 1
The resulting value for $\Delta_f H°_{298}^{DFT-2}$ is $-665.6\,kJ\,mol^{-1}$. As illustrated in Fig. 7, this value is not in full accordance with our assessment, however, the relative difference remains lower than 1%.

### 5. Conclusions

We performed heat capacity measurements with DSC (from ambient to 871 K) and drop calorimetry (from 823 to 1123 K) on synthetic CuCrO$_2$ delafossite samples, as well as DFT calculations at 0 K. Our two sets of experimental data are very consistent. Combined with low temperature literature data, the heat capacity is described from 0 to 1300 K, from which we derive the standard enthalpy at 298 K. A "third law" analysis of 14 *emf* data points provides a mean value for the enthalpy of formation of CuCrO$_2$ at 298 K, which is very consistent with

**Table 5**
Assessed thermodynamic data for CuCrO₂.

| T (K) | $c_p^{\circ}{}_T$ (J K$^{-1}$ mol$^{-1}$) | $H^{\circ}{}_T - H^{\circ}{}_{298}$ (J mol$^{-1}$) | $S^{\circ}{}_T$ (J K$^{-1}$ mol$^{-1}$) | $\Delta_f H^{\circ}{}_T$ (kJ mol$^{-1}$) | $\Delta_f G^{\circ}{}_T$ (kJ mol$^{-1}$) |
|---|---|---|---|---|---|
| 298.15 | 76.51 | 0 | 88.89 | −670800.0 | −619267.6 |
| 300 | 76.76 | 141.8 | 89.36 | −670801.6 | −618947.8 |
| 350 | 82.26 | 4126.6 | 101.64 | −670735.1 | −610308.1 |
| 400 | 86.05 | 8339.8 | 112.89 | −670518.3 | −601689.1 |
| 450 | 88.78 | 12714.1 | 123.19 | −670212.7 | −593103.1 |
| 500 | 90.84 | 17206.9 | 132.65 | −669855.9 | −584554.2 |
| 550 | 92.43 | 21790.1 | 141.39 | −669473.4 | −576042.4 |
| 600 | 93.69 | 26444 | 149.49 | −669082.6 | −567565.9 |
| 650 | 94.70 | 31154.5 | 157.03 | −668696.3 | −559121.9 |
| 700 | 95.54 | 35911.3 | 164.08 | −668323.3 | −550707.2 |
| 750 | 96.24 | 40706.2 | 170.69 | −667970.2 | −542318.5 |
| 800 | 96.83 | 45533.2 | 176.92 | −667642.5 | −533952.6 |
| 850 | 97.33 | 50387.5 | 182.81 | −667344.6 | −525606.2 |
| 900 | 97.76 | 55265.1 | 188.38 | −667080.4 | −517276.5 |
| 950 | 98.14 | 60162.9 | 193.68 | −666853.0 | −508960.4 |
| 1000 | 98.47 | 65078.4 | 198.72 | −666665.3 | −500655.3 |
| 1050 | 98.76 | 70009.3 | 203.53 | −666520.0 | −492358.6 |
| 1100 | 99.02 | 74953.9 | 208.13 | −666419.8 | −484067.7 |
| 1150 | 99.25 | 79910.7 | 212.54 | −666367.1 | −475780.3 |
| 1200 | 99.46 | 84878.4 | 216.77 | −666364.2 | −467494.2 |
| 1250 | 99.64 | 89855.9 | 220.83 | −666413.6 | −459207.1 |
| 1300 | 99.81 | 94842.2 | 224.74 | −666517.5 | −450917.0 |

our value calculated at 0 K by DFT and extrapolated to 298 K.

Based on this assessment, we propose, for the first time, a full set of thermodynamic data for the delafossite phase CuCrO₂. These data, tabulated in Table 5, present a great interest for research and development activities linked to the application of the delafossite materials on a very large range of temperature.

## Appendix A. Supplementary data

Supplementary material related to this article can be found, in the online version, at doi:https://doi.org/10.1016/j.tca.2019.178345.

## References

[1] A. Barnabé, Y. Thimont, M. Lalanne, L. Presmanes, P. Tailhades, p-Type conducting transparent characteristics of delafossite Mg-doped CuCrO₂ thin films prepared by RF-sputtering, J. Mater. Chem. C 3 (2015) 6012–6024, https://doi.org/10.1039/C5TC01070E.

[2] J. Crêpellière, P. Lunca Popa, N. Bahlawane, R. Leturcq, F. Werner, S. Siebentritt, D. Lenoble, Transparent conductive CuCrO₂ thin films deposited by pulsed injection metal organic chemical vapor deposition: up-scalable process technology for an improved transparency/conductivity trade-off, J. Mater. Chem. C 4 (2016) 4278–4287, https://doi.org/10.1039/C6TC00383D.

[3] S. Mahapatra, S.A. Shivashankar, Low-pressure metal–organic chemical vapor deposition of transparent and p-Type conducting CuCrO₂ thin films with high conductivity, Chem. Vap. Depos. 9 (2003) 238–240, https://doi.org/10.1002/cvde.200304147.

[4] A.P. Amrute, Z. Łodziana, C. Mondelli, F. Krumeich, J. Pérez-Ramírez, Solid-state chemistry of cuprous delafossites: synthesis and stability aspects, Chem. Mater. 25 (2013) 4423–4435, https://doi.org/10.1021/cm402902m.

[5] W. Ketir, A. Bouguelia, M. Trari, Visible light induced NO₂-removal over CuCrO₂ catalyst, Water Air Soil Pollut. 199 (2009) 115–122, https://doi.org/10.1007/s11270-008-9864-z.

[6] R. Manickam, K. Biswas, Double doping induced power factor enhancement in

[7] I. Sinnarasa, Y. Thimont, L. Presmanes, A. Barnabé, P. Tailhades, Thermoelectric and transport properties of delafossite CuCrO₂: Mg thin films prepared by RF magnetron sputtering, Nanomaterials (Basel) 7 (2017), https://doi.org/10.3390/nano7070157.

[8] I. Sinnarasa, Y. Thimont, L. Presmanes, C. Bonningue, A. Barnabé, P. Tailhades, Influence of thickness and microstructure on thermoelectric properties of Mg-doped CuCrO₂ delafossite thin films deposited by RF-magnetron sputtering, Appl. Surf. Sci. 455 (2018) 244–250, https://doi.org/10.1016/j.apsusc.2018.05.104.

[9] M. Poienar, F. Damay, C. Martin, J. Robert, S. Petit, Spin dynamics in the geometrically frustrated multiferroic CuCrO₂, Phys. Rev. B 81 (2010) 104411, https://doi.org/10.1103/PhysRevB.81.104411.

[10] S. Seki, Y. Onose, Y. Tokura, Spin-driven ferroelectricity in triangular lattice antiferromagnets ACrO₂ (A = Cu, Ag, Li, or Na), Phys. Rev. Lett. 101 (2008) 067204, https://doi.org/10.1103/PhysRevLett.101.067204.

[11] A.M.M. Gadalla, J. White, The system CuO–Cu₂O–Cr₂O₃ and its bearing on the performance of basic refractories in copper-melting furnaces, Trans. Br. Ceram. Soc. 63 (1964) 535–552.

[12] G.M. Kale, Thermal decomposition of CuCrO₄·2CuO·2H₂O and phase relations in the Cu-Cr-O system, J. Mater. Sci. 30 (1995) 1420–1424, https://doi.org/10.1007/BF00375241.

[13] K.T. Jacob, G.M. Kale, Y. Waseda, Gibbs energy of formation of CuCrO₄ and phase relations in the system Cu-Cr-O below 735 K, Thermochim. Acta 208 (1992) 341–348, https://doi.org/10.1016/0040-6031(92)80176-W.

[14] J. Hamuyuni, P. Taskinen, Liquidus experimental data for the system Cu-O-Cr₂O₃ in air, Thermochim. Acta 638 (2016) 96–102, https://doi.org/10.1016/j.tca.2016.06.020.

[15] P. Perrot, Chromium – copper – oxygen, in: G. Effenberg, S. Ilyenko (Eds.), Refractory Metal Systems: Selected Systems from C-Ta-W to Ti-V-W, Springer, Berlin Heidelberg, 2010, pp. 126–137, , https://doi.org/10.1007/978-3-642-00771-2_9.

[16] K.T. Jacob, G.M. Kale, G.N.K. Iyengar, Oxygen potentials, Gibbs' energies and phase relations in the Cu-Cr-O system, J. Mater. Sci. 21 (1986) 2753–2758.

[17] K.C. Vlach, Y.-Z. You, Y. Austin Chang, A thermodynamic study of the Cu-Cr-O system by the EMF method, Thermochim. Acta 103 (1986) 361–370, https://doi.org/10.1016/0040-6031(86)85173-5.

[18] N.G. Schmahl, E. Minzl, Ermittlung thermodynamischer Daten Von Doppeloxidbildungen aus Gleichgewichtsmessungen, Z. Phys. Chem. 47 (1965) 358–382, https://doi.org/10.1524/zpch.1965.47.5_6.358.

[19] T. Okuda, Y. Beppu, Y. Fujii, T. Onoe, N. Terada, S. Miyasaka, Specific heat of delafossite oxide CuCr₁₋ₓMgₓO₂ (0 ≤ x ≤ 0.03), Phys. Rev. B 77 (2008), https://doi.org/10.1103/PhysRevB.77.134423.

[20] M. Poienar, F. Damay, C. Martin, V. Hardy, A. Maignan, G. André, Structural and magnetic properties of CuCr₁₋ₓMgₓO₂ by neutron powder diffraction, Phys. Rev. B 79 (2009) 014412, https://doi.org/10.1103/PhysRevB.79.014412.

[21] D.O. Scanlon, G.W. Watson, Understanding the p-type defect chemistry of CuCrO₂, J. Mater. Chem. 21 (2011) 3655–3663, https://doi.org/10.1039/C0JM03852K.

[22] K.T. Jacob, A. Kumar, Y. Waseda, Gibbs energy of formation of MnO: measurement and assessment, J. Phase Equilib. Diffus. 29 (2008) 222–230, https://doi.org/10.1007/s11669-008-9280-5.

[23] M. Lalanne, A. Barnabé, F. Mathieu, P. Tailhades, Synthesis and thermostructural studies of a CuFe₁₋ₓCrₓO₂ delafossite solid solution with 0 ≤ x ≤ 1, Inorg. Chem. 48 (2009) 6065–6071, https://doi.org/10.1021/ic900437x.

[24] D.A. Ditmars, S. Ishihara, S.S. Chang, G. Bernstein, E.D. West, Enthalpy and heat-capacity standard reference material: synthetic sapphire (a-$Al_2O_3$) from 10 to 2250 K, J. Res. Bur. Stand. 87 (1982) 159–163.

[25] P. Benigni, G. Mikaelian, R. Pothin, A. Berche, R.M. Ayral, J.C. Tedenac, P. Jund, J. Rogez, Measurement of the heat capacity of ZnSb by DSC between 300 and 673 K, Calphad 55 (2016) 238–242, https://doi.org/10.1016/j.calphad.2016.09.008.

[26] P. Hohenberg, W. Kohn, Inhomogeneous electron gas, Phys. Rev. 136 (1964) B864–B871, https://doi.org/10.1103/PhysRev.136.B864.

[27] W. Kohn, L.J. Sham, Self-consistent equations including exchange and correlation effects, Phys. Rev. 140 (1965) A1133–A1138, https://doi.org/10.1103/PhysRev.140.A1133.

[28] G. Kresse, J. Furthmüller, Efficient iterative schemes for ab initio total-energy calculations using a plane-wave basis set, Phys. Rev. B 54 (1996) 11169–11186, https://doi.org/10.1103/PhysRevB.54.11169.

[29] G. Kresse, D. Joubert, From ultrasoft pseudopotentials to the projector augmented-wave method, Phys. Rev. B 59 (1999) 1758–1775, https://doi.org/10.1103/PhysRevB.59.1758.

[30] J. Sun, A. Ruzsinszky, J.P. Perdew, Strongly Constrained and appropriately normed semilocal density functional, Phys. Rev. Lett. 115 (2015) 036402, https://doi.org/10.1103/PhysRevLett.115.036402.

[31] H.J. Monkhorst, J.D. Pack, Special points for Brillouin-zone integrations, Phys. Rev. B 13 (1976) 5188–5192, https://doi.org/10.1103/PhysRevB.13.5188.

[32] P.E. Blöchl, O. Jepsen, O.K. Andersen, Improved tetrahedron method for Brillouin-zone integrations, Phys. Rev. B 49 (1994) 16223–16233, https://doi.org/10.1103/PhysRevB.49.16223.

[33] V.M. Gurevich, O.L. Kuskov, N.N. Smirnova, K.S. Gavrichev, A.V. Markin, Thermodynamic functions of eskolaite $Cr_2O_3$(c) at 0–1800 K, Geochem. Int. 47 (2009) 1170, https://doi.org/10.1134/S0016702909120027.

[34] M.W. Chase, NIST-JANAF thermochemical tables, J. Phys. Chem. Ref. Data. Monogr. 9 (1998).

[35] J.H. Hu, H.L. Johnston, Low temperature heat capacities of inorganic solids. IX. Heat capacity and thermodynamic properties of cuprous oxide from 14 to 300 K, J. Am. Chem. Soc. 73 (1951) 4550–4551, https://doi.org/10.1021/ja01154a017.

[36] A.D. Mah, L.B. Pankratz, W.W. Weller, E.G. King, Thermodynamic Data for Cuprous and Cupric Oxides, US Dept. of the Interior, Bureau of Mines, 1967, p. 7026.

[37] C.W. Bale, E. Bélisle, P. Chartrand, S.A. Decterov, G. Eriksson, A.E. Gheribi, K. Hack, I.-H. Jung, Y.-B. Kang, J. Melançon, A.D. Pelton, S. Petersen, C. Robelin, J. Sangster, P. Spencer, M.-A. Van Ende, FactSage thermochemical software and databases, 2010–2016, Calphad 54 (2016) 35–53, https://doi.org/10.1016/j.calphad.2016.05.002.

[38] J.W. Arblaster, Thermodynamic properties of copper, J. Phase Equilib. Diffus. 36 (2015) 422–444, https://doi.org/10.1007/s11669-015-0399-x.

[39] A.T. Dinsdale, SGTE data for pure elements, Calphad 15 (1991) 317–425, https://doi.org/10.1016/0364-5916(91)90030-N.

[40] R.J. Corruccini, J.J. Gniewek, Specific Heats and Enthalpies of Technical Solids at Low Temperatures. A Compilation From the Literature, National Bureau of Standards, Washington, D.C, 1960 (Accessed 11 May 2019), https://www.osti.gov/biblio/4803576.

[41] H.W. Woolley, Thermodynamic Properties of Molecular Oxygen, National Bureau of Standards, (1953) (Accessed 23 May 2019), http://archive.org/details/thermodynamicpro2611wool.

[42] J. Leitner, P. Voňka, D. Sedmidubský, P. Svoboda, Application of Neumann–Kopp rule for the estimation of heat capacity of mixed oxides, Thermochim. Acta 497 (2010) 7–13, https://doi.org/10.1016/j.tca.2009.08.002.

[43] T. Zienert, O. Fabrichnaya, Prediction of heat capacity for crystalline substances, Calphad 65 (2019) 177–193, https://doi.org/10.1016/j.calphad.2019.01.017.

[44] A. Maignan, C. Martin, R. Frésard, V. Eyert, E. Guilmeau, S. Hébert, M. Poienar, D. Pelloquin, On the strong impact of doping in the triangular antiferromagnet $CuCrO_2$, Solid State Commun. 149 (2009) 962–967, https://doi.org/10.1016/j.ssc.2009.02.026.

[45] Working Group 1 of the Joint Committee for Guides in Metrology, Evaluation of Measurement Data — Guide to the Expression of Uncertainty in Measurement, (2008) (Accessed 12 April 2019), https://www.bipm.org/utils/common/documents/jcgm/JCGM_100_2008_E.pdf.

[46] L.M. Corliss, J.M. Hastings, R. Nathans, G. Shirane, Magnetic structure of $Cr_2O_3$, J. Appl. Phys. 36 (1965) 1099–1100, https://doi.org/10.1063/1.1714118.